

## Case study of a tornado in the Upper Rhine valley

Ronald Hannesen, Nikolai Dotzek, Hermann Gysi, and Klaus D. Beheng

FZK–Institut für Meteorologie und Klimaforschung,  
Postfach 3640, D–76021 Karlsruhe, Germany

*Received 5 November 1997, in final form 2 February 1998*

### Corresponding author's address:

Dr. R. Hannesen

Gematronik GmbH

Raiffeisenstr. 10, D–41470 Neuss–Rosellen, Germany.

E-mail: [r.hannesen@gematronik.com](mailto:r.hannesen@gematronik.com),

Tel: +49–2137–782–0, Fax: +49–2137–782–11.

# Case study of a tornado in the Upper Rhine valley

Ronald Hanesen, Nikolai Dotzek, Hermann Gysi, and Klaus D. Beheng

FZK–Institut für Meteorologie und Klimaforschung,

Postfach 3640, D–76021 Karlsruhe, Germany

**Summary.** On 9 September 1995 a short-lived tornado occurred in the Upper Rhine valley near Oberkirch–Nußbach, uprooting several trees as well as damaging buildings and cars. The storm, confirmed by eye witnesses and damage analyses performed by Wetteramt Freiburg of the German Weather Service, was also detected by the IMK C–band Doppler radar in Karlsruhe. The data show a well-defined mesocyclonic rotation in the tornado’s parent Cb cloud. The orography distinctly influenced the development of a wind field suitable for supercell formation. This points to preferred areas of tornadic activity. The dominant effects of vertical wind shear compared to convective energy during tornadogenesis are evident for this storm. Its small scale confirms the existence of small supercell storms being studied in the USA in recent years.

## Fallstudie eines Tornados im Oberrheingraben

**Zusammenfassung.** Am 9. September 1995 bildete sich im Oberrheingraben bei Oberkirch–Nußbach ein kurzlebiger Tornado, der eine größere Anzahl von Bäumen entwurzelte sowie Gebäude und Autos beschädigte. Der durch Augenzeugenberichte und Schadenanalysen des Wetteramts Freiburg belegte Tornado ist auch in den Daten des IMK C–Band Doppler–Radars in Karlsruhe nachzuweisen. Die Beobachtungen belegen eine ausgeprägte Mesozylone in der Cb–Mutterwolke des Tornados. Die Orographie hat die Ausbildung eines für Superzellen–Entstehung günstigen Strömungsfeldes entscheidend beeinflusst, was einen Hinweis auf bevorzugte Tornadogebiete im Oberrheingraben liefert. Bei diesem Sturm dominierte bei der Tornadogenese die vertikale Windscherung gegenüber der potentiellen Auftriebsenergie. Seine geringe Ausdehnung untermauert die Existenz der kleinen Superzellen–Gewitter, die in den USA seit einigen Jahren studiert werden.

# 1 Introduction

In the Tornado and Storm Research Organization TORRO<sup>1</sup> statistics of 1995, two tornadoes in southern Germany are recorded (26/27 January and 9 September 1995), yet still lacking distinct meteorological confirmation.

Whereas the report on the January event is rather sketchy and could not be corroborated by newspaper articles, inquiries at forest authorities and by other sources, the event of September 1995 could be verified. The tornado occurred near Oberkirch–Nußbach and was confirmed by eye witnesses and newspaper articles as well as by damage analyses from the German Weather Service (DWD), performed by Wetteramt Freiburg (DWD 1995a). The event was also recognized in the data obtained by a C-band Doppler radar located 70 km north of the tornado site at the Institute for Meteorology and Climate Research in Karlsruhe (IMK). Due to the small distance between the tornado and the radar, detailed analyses of that particular tornadic storm could be performed. The results of these investigations are presented here. As a main point it is anticipated that the orography of the Rhine valley area strongly influenced the development of the small supercell storm towards its tornadic phase.

The article is divided into the following sections: in Sec. 2 a brief general overview on weather conditions which may lead to tornadic activity in the Upper Rhine valley is given. The synoptic setting of 9 September 1995 including a description of the tornado is outlined in Sec. 3. Analysis of the radar data is presented in Sec. 4 and (thermo-) dynamic processes during the vortex development are identified. The results are discussed in Sec. 5 and related to other recorded tornadic events in the central region of the Upper Rhine valley.

## 2 Conditions for tornadogenesis

This section gives a brief and exemplary overview on typical weather factors which favor tornadogenesis in the Upper Rhine valley region during the warm season and relates them to relevant meteorological parameters. For a broader description of thunderstorms, especially supercells exhibiting mesocyclonic rotation and tornadogenesis the reader is referred to Klemp (1987) and Houze (1993).

Data analysis of recorded tornadoes from past decades reveals that during the summer

---

<sup>1</sup><http://www.torro.org.uk/>

months tornadic storms in the Upper Rhine valley region are most probable if warm and moist air from the Mediterranean or from central Spain is advected across southern France (the “Spanish plume” (Morris 1986)) through the Rhône valley, the Swiss Jura mountains and the Belfort Gap<sup>2</sup> into the Rhine valley (cf. Dessens and Snow 1989). If the synoptic conditions prevail and the advected air mass ages, the low-level moisture content rises in the Rhine valley due to evapotranspiration with limited vertical mixing below a low-level inversion at a typical height of about 1.5 km. Simultaneously, the temperature increases from day to day due to strong input of solar radiation. As a consequence the low-level equivalent potential temperature,  $\Theta_e$ , continuously attains larger values.

Lifting at a cold front approaching from W–NW or positive vorticity advection with the passage of a short-wave upper level trough may remove the inversion layer above the near-surface high- $\Theta_e$  air and induce deep moist convection. Another ingredient necessary for severe convection triggering tornadogenesis is the occurrence of strong mid- or upper-tropospheric winds veering with height, e. g. low-level southerly winds and a westerly jet stream (Weisman and Klemp 1984).

In the Upper Rhine valley the directional wind shear is strongest near the top of the boundary layer. This is caused by a specific interaction of airflow and orography: the boundary-layer air is channeled along the valley between the Vosges and the Black Forest, leading to southerly flow in the lowest  $\approx 0.5$  km of the atmosphere (Adrian and Fiedler 1991). In higher levels the flow regime is considerably influenced by another orographic feature: between the Vosges and Palatinian mountains the saddle-like depression of Saverne leads to an enhanced westerly flow above  $\approx 0.5$  km. This flow system is supported by the terrain west of the Saverne depression gently rising eastward, thus gradually accelerating the westerly winds. Farther into the Rhine valley a convergence line forms, separating the air masses with westerly higher-level and southerly boundary-layer winds. This results in a large low-level shear situation which may continue in the vertical. The hodograph then displays veering winds becoming stronger with height, a necessary condition for supercell formation as stated above.

If the abovementioned synoptic and meso-meteorological setting occurs during the warm season, severe thunderstorms producing hail and sometimes spawning tornadoes are likely to develop in the Upper Rhine valley region. The strong Pforzheim tornado of 10 July 1968 is an

---

<sup>2</sup>For a depiction of geographical names cf. Fig. 1 showing the orography surrounding the radar with range rings added at 30 km intervals.

impressive example of such a situation (Nestle 1969).

The probability of supercellular storms can be estimated by several parameters (cf. Weisman and Klemp 1984, Brooks et al. 1994):

- convective available potential energy CAPE

$$\text{CAPE} = g \int_{\text{LFC}}^{\text{LNB}} \frac{\Theta_v - \bar{\Theta}_v}{\bar{\Theta}_v} dz$$

defining an upper limit of potential energy due to buoyancy forces available to an air parcel rising from the level of free convection, LFC, to the level of neutral buoyancy, LNB. While  $\Theta_v$  denotes virtual potential temperature of the ascending parcel,  $\bar{\Theta}_v$  corresponds to an environmental sounding. Note that CAPE is strongly dependent on the near-surface values of  $\Theta_v$ .

- bulk–Richardson number  $Ri_b$

$$Ri_b = 2 \frac{\text{CAPE}}{(\mathbf{v}_l - \mathbf{v}_m)^2}$$

estimating the degree to which the moist convection is dynamically or thermodynamically dominated. The wind vectors  $\mathbf{v}_l$  and  $\mathbf{v}_m$  refer to low and mid-tropospheric levels, respectively.

- storm–relative helicity SRH

$$\text{SRH} = - \int_0^H \mathbf{e}_z \cdot (\mathbf{v} - \mathbf{c}) \times \partial_z \mathbf{v} dz$$

indicating helical components of the storm–relative flow field in the vertical. Positive SRH corresponds to cyclonic sense of rotation. While  $\mathbf{c}$  is the storm motion and  $\mathbf{v}$  the environmental wind vector,  $H$  is that particular level between ground and  $\approx 3$  km which yields the largest SRH. Closely related to SRH is the criterion that a supercell storm may occur if the hodograph shows veering winds with height and a storm motion vector  $\mathbf{c}$  situated to the right of the hodograph.

- energy–helicity index EHI

$$\text{EHI} = \frac{\text{CAPE} \times \text{SRH}}{\text{EHI}_0}$$

accounting for the probability of strong ( $\text{EHI} > 1$ ) or violent tornadoes ( $\text{EHI} > 2.5$ ) for an empirical reference value  $\text{EHI}_0$ . For Great Plains tornadoes in the USA  $\text{EHI}_0 = 1.6 \times 10^5 \text{ J}^2 \text{ kg}^{-2}$  is assumed.

### 3 Synoptic conditions and storm parameters

On 9 September 1995 the synoptic setting was similar to the situation described above. South-western Germany was influenced by a deep low centered about 500 km farther north which had originated from tropical hurricane Iris. A weak cold front had already passed the region under consideration, but on the low's southern flank warm and moist air still moved into the south-western parts of Germany. Fig. 2 shows the corresponding surface analysis of 00:00 UTC (adapted from DWD 1995b). A mid-tropospheric trough passed the area around noon increasing the atmospheric instability. A cold pool over the Upper Rhine valley can be inferred from the relative topography 50/100 kPa–chart of 12:00 UTC (not shown here).

In the unstably stratified air mass several rain showers developed over south-western Germany; a few thunderstorms were also observed. At 12:55 LST (local standard time, 10:55 UTC) one of these storms spawned a tornado near Oberkirch–Nußbach located at the eastern flank of the Upper Rhine valley. The funnel was observed by several persons. In the region affected many large apple and plum trees were uprooted and thrown away up to 20 m. Shingles were blown down from some Nußbach houses, damaging cars. The tornado swath was about 1 km long and 50 m wide. From the trees' fall pattern a counterclockwise rotating vortex could be reconstructed (DWD 1995a). According to the TORRO and Fujita intensity scales (Meaden 1976, Fujita 1981) the reported damages indicate a T2/F1 tornado intensity, i. e. a weak tornado.

For calculating the various storm parameters a complete set of meteorological data near the tornado site is required. The data used were those of the 13:00 LST rawinsonde ascent from Stuttgart located  $\approx$  90 km east of Nußbach at 330 m ASL as well as those of the IMK 200 m mast and the C-band Doppler radar, both located 10 km north of Karlsruhe and 70 km north of Nußbach at 110 m ASL (cf. Fig. 1).

Mast temperature and dewpoint data are added to the Stuttgart sounding to consider near-surface meteorological variables in the Upper Rhine valley. This procedure leads to the profiles shown in Fig. 3. The importance of the near-surface values turns out in calculating CAPE: using the Stuttgart sounding only, CAPE amounts to  $70 \text{ J kg}^{-1}$  whereas taking the mast data in the lowest levels into account yields a CAPE of  $440 \text{ J kg}^{-1}$  with  $LFC = 1.3 \text{ km}$  and  $LNB = 7.3 \text{ km}$  ASL<sup>3</sup>.

The profiles of horizontal wind speed and direction in Fig. 3 given by the Stuttgart rawin-

---

<sup>3</sup>For the Upper Rhine valley region considered here, ASL  $\approx$  AGL + 110 m.

sonde data and calculated from IMK Doppler radar data by the VVP (volume velocity processing)–method (Waldteufel and Corbin 1979) show increasing winds veering with height in the lowest 3 km. A hodograph representative for the Upper Rhine valley region can be obtained by using IMK mast and radar data for lower levels and Stuttgart rawinsonde data for upper heights where no radar data are available due to a lack of echoes. The result is shown in Fig. 4 by the solid line. The shear vector continuously veers with height establishing a situation suitable for the development of storms with embedded counterclockwise rotating mesocyclones (Weisman and Klemp 1984). Denoted by the asterisk in Fig. 4 is the storm motion vector. Evaluating the wind profile leads to a SRH of  $105 \text{ J kg}^{-1}$  and EHI  $\approx 0.3$ , values typically found in the environment of weak tornadoes (Kerr and Darkow 1996). The obtained  $Ri_b$  of 25 is further evidence for possible supercell thunderstorm formation (Weisman and Klemp 1984).

For comparison Fig. 4 also shows the low–level winds of the Stuttgart sounding (dashed line). That hodograph is of a more straight–line type with the storm motion vector lying very close to it. The resulting Stuttgart values of  $\text{SRH} = -4 \text{ J kg}^{-1}$  and  $\text{EHI} \approx -0.002$  provide no evidence for any possible supercell thunderstorms.

## 4 Analysis of Doppler radar data

Since January 1994 operational C–band Doppler radar measurements are performed at IMK, comprising polar volume radar reflectivity and Doppler velocity values in 16 elevations within a range of 120 km every 10 to 12 min (see Gysi (1995) for a detailed description of the radar).

Figs. 5 and 6 provide valuable information of the storm development. For 12:33, 12:45, and 12:57 LST, respectively, Figs. 5 a–c show reflectivity PPIs within the area marked by the rectangle in Fig. 1 at an elevation of 1.5 deg corresponding to an altitude of roughly 2.5 km ASL. The development of an intense precipitation core can clearly be seen with the reflectivity partially exceeding 50 dBZ. However, the hook echo being typical of tornadic supercells was not observed. This may be due to either the small size of the storm or the limited spatial and temporal radar data resolution. Fig. 6 is an echotop display showing the top height of the 40 dBZ plane at different times. Its fast lifting to more than 4 km ASL further proves the existence of strong updrafts within the cloud. Closely resembling the temporal evolution of the 40 dBZ echotop, radar–detected cloud tops reached heights of about 8 km. This is in good agreement with the LNB of 7.3 km given above.

Figs. 7 a–d show Doppler velocity PPIs (Plan Position Indicator) within the area marked by the rectangle in Fig. 1 for 12:40 LST at elevations of 0.2, 1.0, 2.0 and 3.0 deg, corresponding to heights of about 1.0, 2.0, 3.1 and 4.3 km ASL, respectively. The environmental wind velocities and directions in these heights (SW–W flow of roughly  $15 \text{ m s}^{-1}$ , cf. Fig. 3) result in Doppler velocities of about  $-10 \text{ m s}^{-1}$  (i. e. towards the radar). This superposed mean flow component is given by the vertically hatched area in Fig. 7. Considering deviations from this mean flow, the vortex signature typical of a counterclockwise rotating mesocyclone (Donaldson 1970, Doviak and Zrnić 1984) is visible in the PPIs of the lowest 3 elevations (Figs. 7 a–c) by pairwise locations of positive and negative Doppler velocity deviations centered roughly on the 75 km range ring. The deviation extrema are separated by about 3 km and their difference equals  $15 \text{ m s}^{-1}$ . This yields a mean shear of  $0.005 \text{ s}^{-1}$ ; a value sufficient for recognition of significant mesocyclonic vortex signatures as defined e. g. by Linder and Schmid (1996). The vortex signature has a vertical extent of about 3 km and is centered roughly 10 km west of Nußbach<sup>4</sup>. A tornado had not been observed at that time. Fig. 7 d shows that at a height of about 4.3 km the vortex signature no longer exists. Instead, a divergence signature appears: closer to the radar, the Doppler velocity component towards the radar is larger than farther away. This divergence in the upper cloud parts implies an updraft within the mesocyclone underneath, consistent with the reflectivity analysis given above.

Fig. 8 shows the same scan area as Fig. 7 at an elevation of 1.0 deg 12 min later (12:52 LST); shortly before the tornado was observed at Nußbach. The vortex signature is still present, but superposed by a convergence signature: the area of positive Doppler velocity deviation is located a little closer to the radar than the area of negative deviation. A convergence-caused horizontal shrinking and vertical stretching of the vortex may finally have initiated the tornado.

The intensification of the mesocyclone and the tornado touchdown are in phase with a maximum of updraft intensity, apparent from the temporal evolution of the 40 dBZ echotop. It is therefore suggested that vortex-stretching below the overshooting cloud top is the main source for the increase of vorticity and helicity prior to formation of the tornado vortex. A similar case of a mesocyclone with a fast development and vertical extension of high reflectivity areas has also been found by Linder and Schmid (1996) investigating a tornadic storm that struck northern Switzerland on 22 July 1995. On this day, severe thunder- and hailstorms occurred throughout

---

<sup>4</sup>Due to the smallness of this mesovortex the term “misocyclone” as proposed by Fujita (1981) would be more appropriate. For simplicity, only the more common expression “mesocyclone” is used in this paper.

the Rhine valley as well, but no further tornadoes were reported.

For completeness we mention that 3 additional mesocyclones aside from the one of the Nußbach storm were detected on 9 September 1995. Some of these showed even more distinct vortex signatures leading to a mean shear of about  $0.007 \text{ s}^{-1}$ . However, neither were additional tornadoes observed nor did the responsible forest authorities get any information on extraordinary wind damage. Fig. 9 shows the tracks and the times of initiation and decay of the 4 mesocyclones of 9 September 1995. These mesocyclones were identified in the Doppler radar data by vortex signatures embedded within persistent single updrafts beneath regions of upper-level horizontal divergence. All these cases have the following features in common: *i*) the mesocyclones developed in a region between Rastatt and Strasbourg, and *ii*) they formed inmidst the valley's flat region, propagated eastward and decayed soon after reaching the hilly terrain of the northern Black Forest. In the remainder of the radar's observation area, however, containing almost the complete Upper Rhine valley and large areas of the surrounding mountainous regions, no other vortex signatures were found.

## 5 Discussion

In this case study the (thermo-)dynamic processes responsible for the formation of a tornado near the eastern flank of the Upper Rhine valley were investigated by use of a C-band Doppler radar and rawinsonde data. The results show that the thunderstorm spawning the tornado was a small supercell with a well-defined mesocyclone at lower levels and divergence at higher levels of the Cb cloud. This can be attributed to a strong upward-directed convective mass flux through the updraft core of the storm.

Mostly undisturbed by orographic effects, the storm developed above the relatively flat terrain of the Rhine valley for the transition to the tornadic phase, while the downward generation of the funnel was facilitated by a low-level vorticity increase above the upsloping terrain at the eastern flank of the valley. However, the small supercell was too weak to maintain the tornado vortex on its way to the hilly terrain of the northern Black Forest for longer times. In effect, the tornado persisted for only a few minutes and the supercell also disappeared about 15 min later.

The radar-observed cloud tops at  $\approx 8 \text{ km ASL}$  fit well in the analysis of atmospheric stratification considering the special heat and moisture conditions in the Rhine valley. Typical supercell features were observed with the Nußbach storm. However, both the vertical extent and the

horizontal dimension of the mesocyclone show that the storm was about a factor of 2 smaller than classical Great Plains supercells. In the USA these “mini”–supercellular storms have been observed as well (Kennedy et al. 1993).

The rather small value of CAPE supports analyses of Kerr and Darkow (1996), limiting the main role of CAPE to the strength of convective initiation while stressing the relevance of storm–relative winds and helicity for further evolution to a tornadic supercell. Accordingly the Upper Rhine valley, especially the region in the vicinity of Baden–Baden and Rastatt, is well-suited for the formation and intensification of supercells due to convergence of a channeled boundary–layer flow and the presence of high– $\Theta_e$  air in the Rhine valley as well as mid–level cross–flow enhanced by the Saverne depression as discussed above. The influence of the larger–scale orography is also important since some of those storms developing into supercells do not form in the Rhine valley itself, but have their “nuclei” over the gently eastward upsloping terrain of the high plains of Lorraine (west of the Saverne depression). This is in agreement with investigations on the intensification and growing organization of convection over upsloping terrain (Smith and Yau (1987), Dessens and Snow (1989)) as well as with suggestions by Schaaf et al. (1988) on the initiation of “convection nuclei” induced by certain orographic features.

Therefore the central region of the Upper Rhine valley seems to be a preferred areal for non–tornadic supercell storms. Due to strong wind shears and  $\Theta_e$ –gradients near the convergence line of air masses channeled by both the depression of Saverne and the Rhine valley it is also likely that tornadic supercells occur. Although the results are preliminary and need further research, it is supported by Fig. 10 in which the tracks of the 9 September 1995 mesocyclones and the damage swaths of several tornadoes from past decades are depicted. An accumulation of tornadic events along a well–defined tornado–alley becomes apparent.

## Acknowledgments

The authors are grateful to Willi Schmid of ETH Zürich for his valuable advice on the analysis and noise correction of the Doppler data as well as for comments on this paper. Wilhelm Benz from Nußbach kindly provided us with information and photographs concerning the tornado damage. Thanks to Martin Löffler–Mang for critical proofreading of the text and to an anonymous referee for valuable comments.

## References

- Adrian G., F. Fiedler, 1991: Simulation of unstationary wind and temperature fields over complex terrain and comparison with observations. — *Contr. Atmos. Phys.* **64**, 27–48.
- Brooks H. E., C. A. Doswell, J. Cooper, 1994: On the environments of tornadic and nontornadic mesocyclones. — *Wea. Forecasting* **9**, 606–618.
- Dessens J., J. T. Snow, 1989: Tornadoes in France. — *Wea. Forecasting* **4**, 110–132.
- Donaldson, R. J. Jr., 1970: Vortex signature recognition by a Doppler radar. — *J. Appl. Meteorol.* **9**, 661–670.
- Doviak, R. J., D. S. Zrnić, 1984: *Doppler Radar and Weather Observations*. — Academic Press, New York, 458 pp.
- DWD, 1995a: Wetterkarte. — *Amtsblatt des Deutschen Wetterdienstes* D 7311 A, Jahrgang 1995, Beilage Nr. 138/1995. — Eigenverlag des Deutschen Wetterdienstes, Offenbach.
- DWD, 1995b: *Europäischer Wetterbericht*. — *Amtsblatt des Deutschen Wetterdienstes* D 6168 A, Jahrgang 20, Nr. 252. — Eigenverlag des Deutschen Wetterdienstes, Offenbach.
- Fujita, T. T., 1981: Tornadoes and downbursts in the context of generalized planetary scales. — *J. Atmos. Sci.* **38**, 1511–1534.
- Gysi, H., 1995: Niederschlagsmessung mit Radar in orographisch gegliedertem Gelände. — Diss., Univ. Karlsruhe, 188 S.
- Houze R. A. Jr., 1993: *Cloud Dynamics*. — *Int. Geophys. Ser.* **53**, Academic Press, San Diego, 573 pp.
- Kennedy P. C., N. E. Westcott, R. W. Scott, 1993: Single-Doppler radar observations of a mini-supercell tornadic thunderstorm. — *Mon. Wea. Rev.* **121**, 1860–1870.
- Kerr B. W., G. L. Darkow, 1996: Storm-relative winds and helicity in the tornadic thunderstorm environment. — *Wea. Forecasting* **11**, 489–505.
- Klemp J. B., 1987: Dynamics of tornadic thunderstorms. — *Annu. Rev. Fluid Mech.* **19**, 369–402.

Linder, W., W. Schmid, 1996: A tornadic thunderstorm in Switzerland exhibiting a radar-detectable low-level vortex. — Proc. 12<sup>th</sup> Int. Conf. on Clouds and Precip., Zürich, 577–580.

Meaden G. T., 1976: Tornadoes in Britain: their intensities and distribution in space and time. — J. Meteorol. **1**, 242–251.

Morris R. M., 1986: The Spanish plume — testing the forecaster's nerve. — Meteorol. Mag. **115**, 349–357.

Nestle R., 1969: Der Tornado vom 10. 7. 1968 im Raum Pforzheim. — Meteorol. Rdsch. **22**, 1–3.

Schaaf C. B., J. Wurman, R. M. Banta, 1988: Thunderstorm-producing terrain features. — Bull. Amer. Meteorol. Soc. **69**, 272–277.

Smith S. B., M. K. Yau, 1987: The mesoscale effect of topography on the genesis of Alberta hailstorms. — Contr. Atmos. Phys. **60**, 371–392.

Waldteufel, P., H. Corbin, 1979: On the analysis of single Doppler data. — J. Appl. Meteorol. **18**, 532–542.

Weisman, M. L., J. B. Klemp, 1984: The structure and classification of numerically simulated convective storms in directionally varying wind shears. — Mon. Wea. Rev. **112**, 2479–2498.

Ronald Hannesen

Nikolai Dotzek

Hermann Gysi

Klaus D. Beheng

Institut für Meteorologie und Klimateforschung

Forschungszentrum / Universität Karlsruhe

Postfach 3640

D-76021 Karlsruhe

Germany

Received 5 November 1997, in revised form: 2 February 1998

## Figure captions

Figure 1: Orography surrounding the Doppler radar. Marked boxes indicate the areas of Figs. 5, 7 and 8 (small rectangle) and 9 (square). Locality names used in the text are included. BB = Baden–Baden, Ffm = Frankfurt, Fr = Freiburg, Ka = Karlsruhe, N = Nußbach, Pf = Pforzheim, Ra = Rastatt, Sb = Saarbrücken, Stg = Stuttgart, Str = Strasbourg, Wü = Würzburg.

Abb. 1: Orographie in der Umgebung des Doppler–Radars. Die gekennzeichneten Ausschnitte entsprechen den Bereichen der Abb. 5, 7 und 8 (kleines Rechteck) sowie 9 (Quadrat).

Figure 2: Surface analysis chart of 00:00 UTC (02:00 LST), 9 September 1995. For details see text.

Abb. 2: Bodenwetterkarte vom 9. September 1995, 00:00 UTC (02:00 LST). Nähere Erläuterungen im Text.

Figure 3: Wind and temperature profiles of 9 September 1995 at 13:00 LST. Data from the Stuttgart rawinsonde supplemented by IMK meteorological mast and Doppler radar data.

Abb. 3: Wind- und Temperaturprofile vom 9. September 1995 um 13:00 LST. Radiosondendaten von Stuttgart, ergänzt um Werte vom meteorologischen Meßmast und vom Doppler–Radar des IMK.

Figure 4: Hodograph of the wind data shown in Fig. 3 for the Upper Rhine valley region (solid line) and the Stuttgart sounding (dashed line). Numbers at the dots represent heights in km ASL. The asterisk marks the storm motion vector.

Abb. 4: Hodogramm der Winddaten aus Abb. 3 für den mittleren Oberrheingraben (ausgezogene Linie) und die Stuttgarter Sondierung (gestrichelt). Die Zahlen an den Punkten geben die Höhe ü. NN in km an. Der Stern markiert die Verlagerungsgeschwindigkeit der Mesozyklone.

Figure 5: PPI of radar reflectivity at an elevation of 1.5 deg for a) 12:33, b) 12:45, and c) 12:57 LST. N = Nußbach.

Abb. 5: PPI der Reflektivität bei einer Elevation von 1,5 Grad um a) 12:33, b) 12:45 und c) 12:57 LST.

Figure 6: Temporal variations of 40 dBZ reflectivity echotop (in km ASL). N = Nußbach.

Abb. 6: Zeitlicher Verlauf der Obergrenze (in km ü. NN) der 40 dBZ–Fläche (Echotop–Darstellung).

Figure 7: PPI of Doppler velocity for 12:40 LST at elevations of a) 0.2 deg, b) 1.0 deg, c) 2.0 deg and d) 3.0 deg. Velocity values are indicated by hatched areas as given by the insert. N = Nußbach.

Abb. 7: PPI der Doppler–Geschwindigkeit um 12:40 LST bei den Elevationen a) 0,2 Grad, b) 1,0 Grad, c) 2,0 Grad und d) 3,0 Grad. Geschwindigkeiten sind durch die in der Legende gezeigten Schraffuren gekennzeichnet.

Figure 8: PPI of Doppler velocity as in Fig. 7 b (at elevation 1.0 deg), but for 12:52 LST.

Abb. 8: PPI der Doppler–Geschwindigkeit wie in Abb. 7 b (Elevation 1,0 Grad), jedoch für 12:52 LST.

Figure 9: Tracks of radar–detected mesocyclones on 9 September 1995. Times correspond to respective first and last radar scans revealing mesocyclonic in–cloud rotation and upper–level divergence signatures. Str = Strasbourg, Ra = Rastatt, BB = Baden–Baden, N = Nußbach.

Abb. 9: Zugbahnen der am 9. September 1995 aufgetretenen Mesozyklonen. Die Zeiten geben jeweils deren erste bzw. letzte Radar–Detektierung an.

Figure 10: Ground tracks of radar-detected mesocyclones on 9 September 1995 (thin lines) and damage swaths of tornadoes (thick lines) in the central region of the Upper Rhine valley. Numbers at tracks correspond to dates of occurrence: 1.) 4 Jul 1885, 2.) 7 Jun 1952, 3.) 27 Apr 1960, 4. a, b) 10 Jul 1968, 5.) 8 May 1985, 6.) 23 Jul 1986, 7.) 21 Jul 1992, 8. a-d) 9 Sep 1995. N = Nußbach, Pf = Pforzheim, Stg = Stuttgart, Str = Strasbourg.

Abb. 10: Zugbahnen der Mesozyklonen des 9. September 1995 (dünne Linien) und verschiedener Tornados (dicke Linien) im mittleren Oberrheingraben.

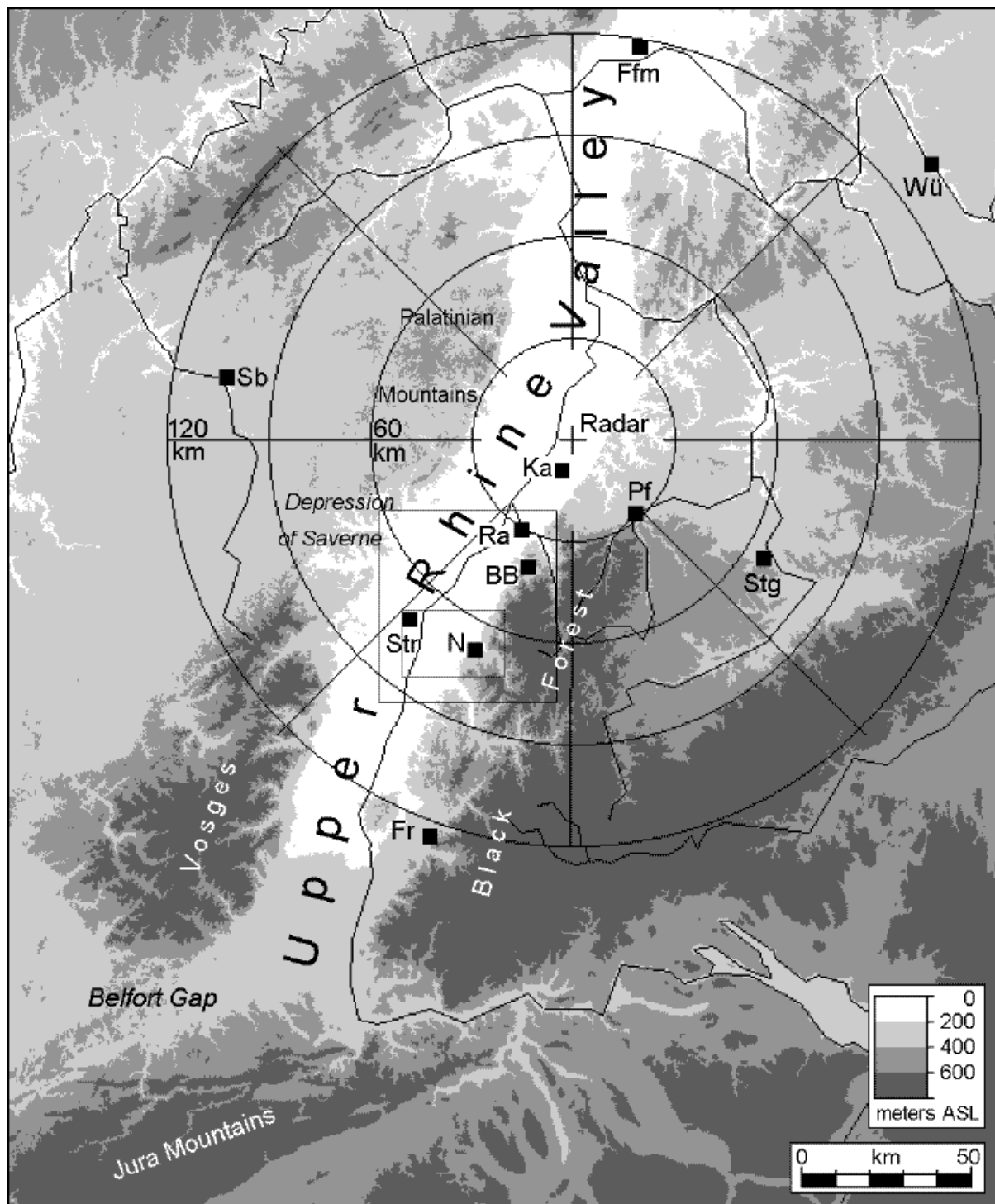


Figure 1

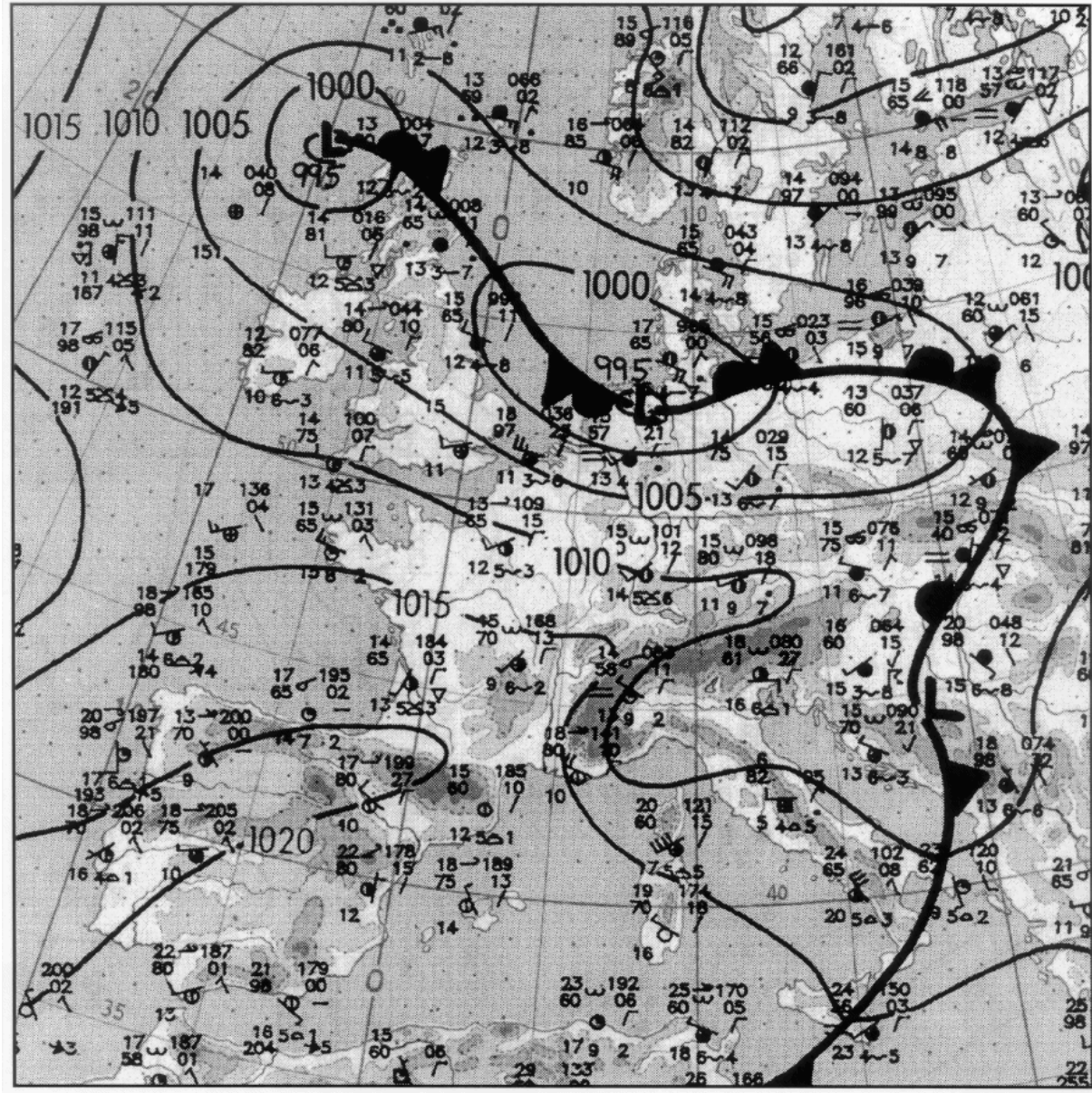


Figure 2

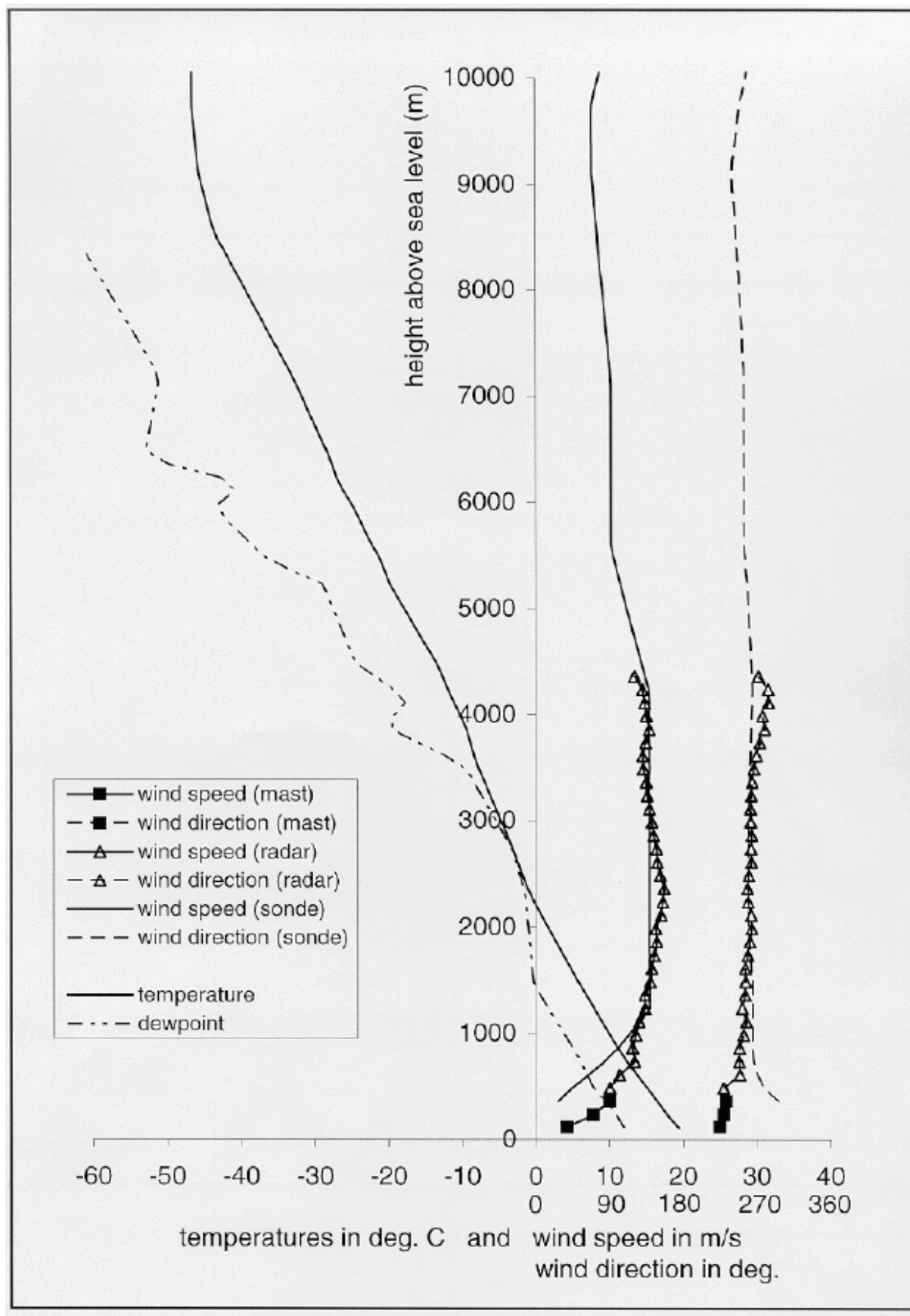


Figure 3

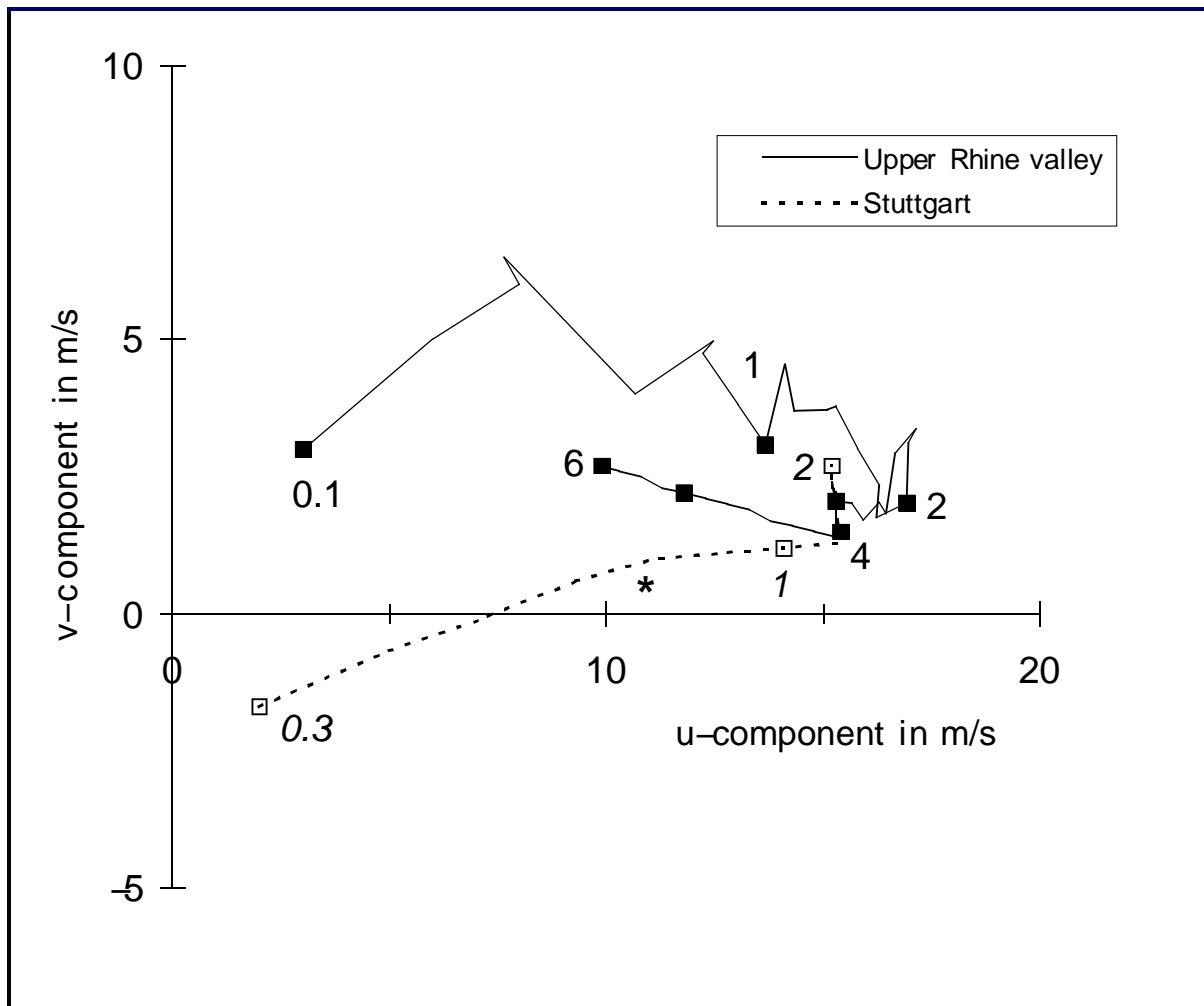


Figure 4

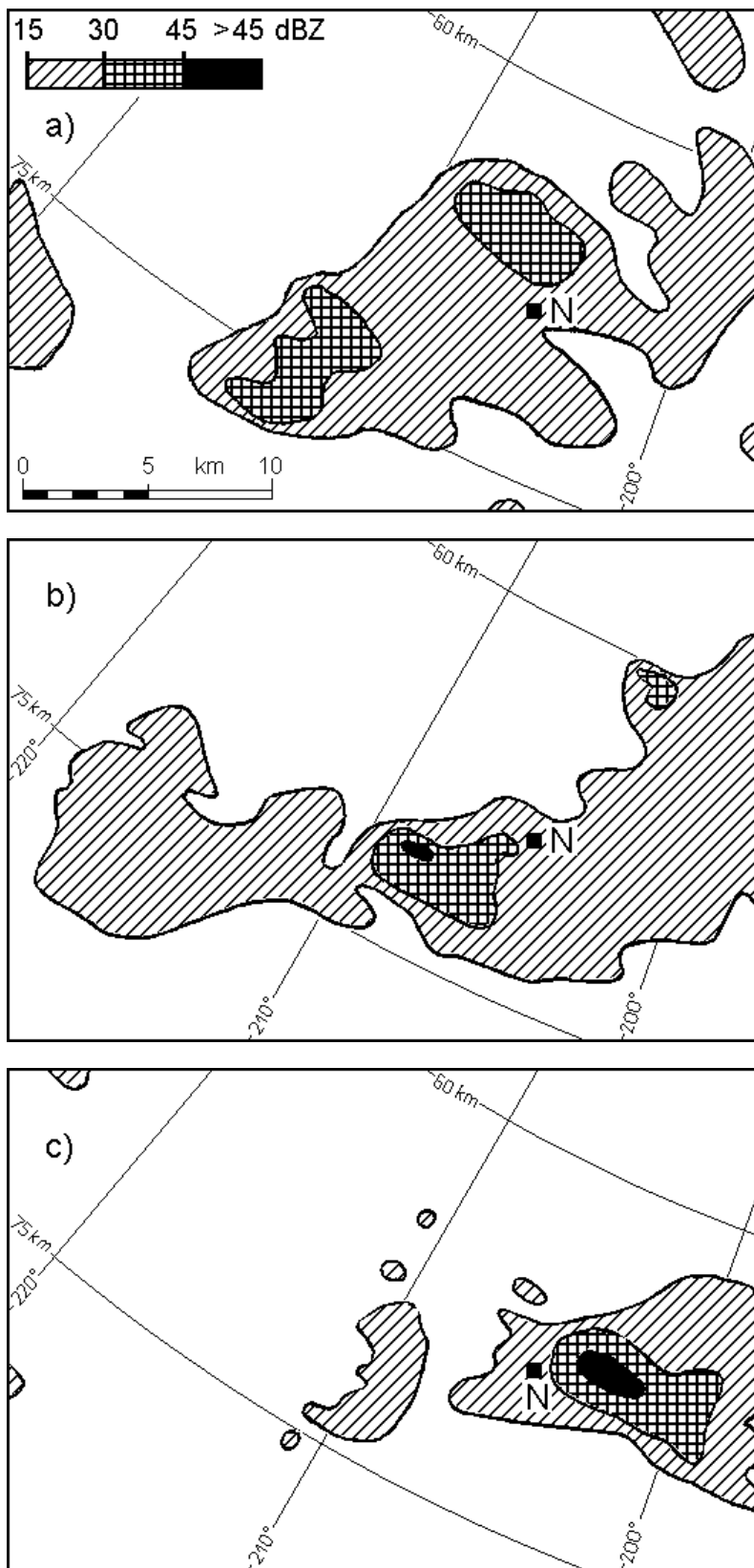


Figure 5

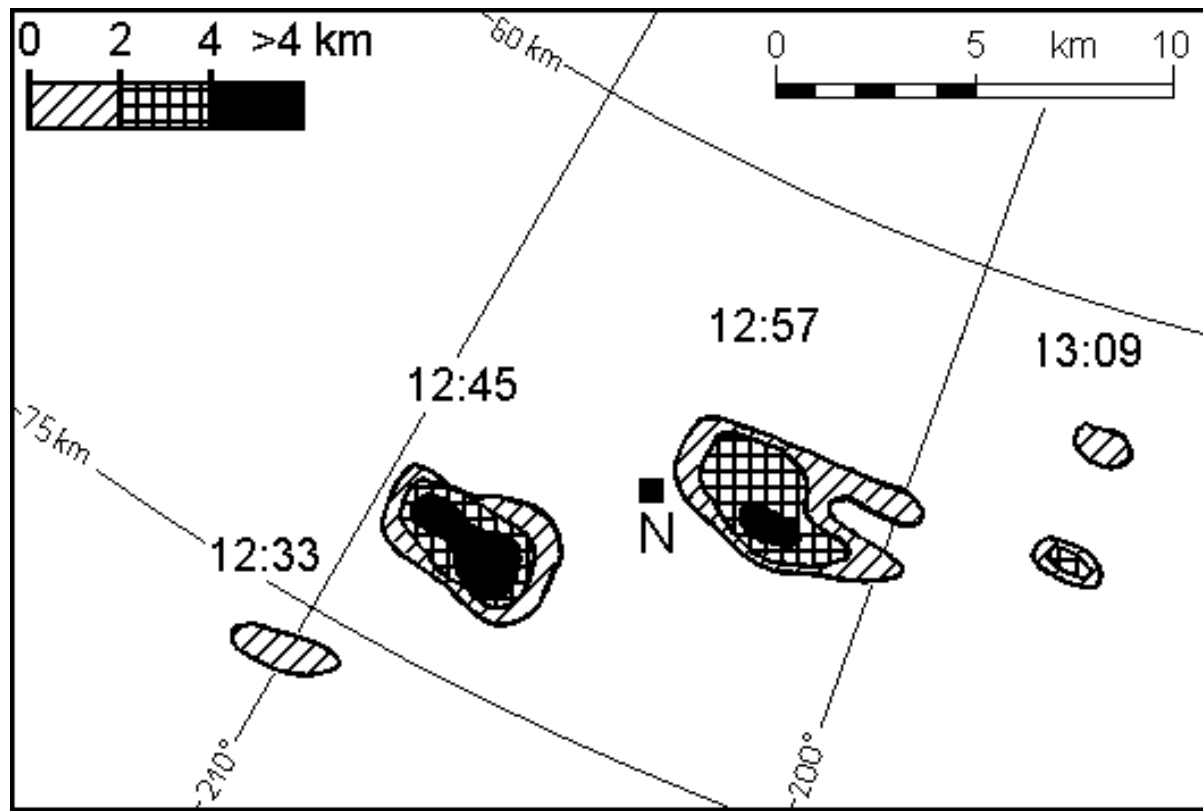


Figure 6

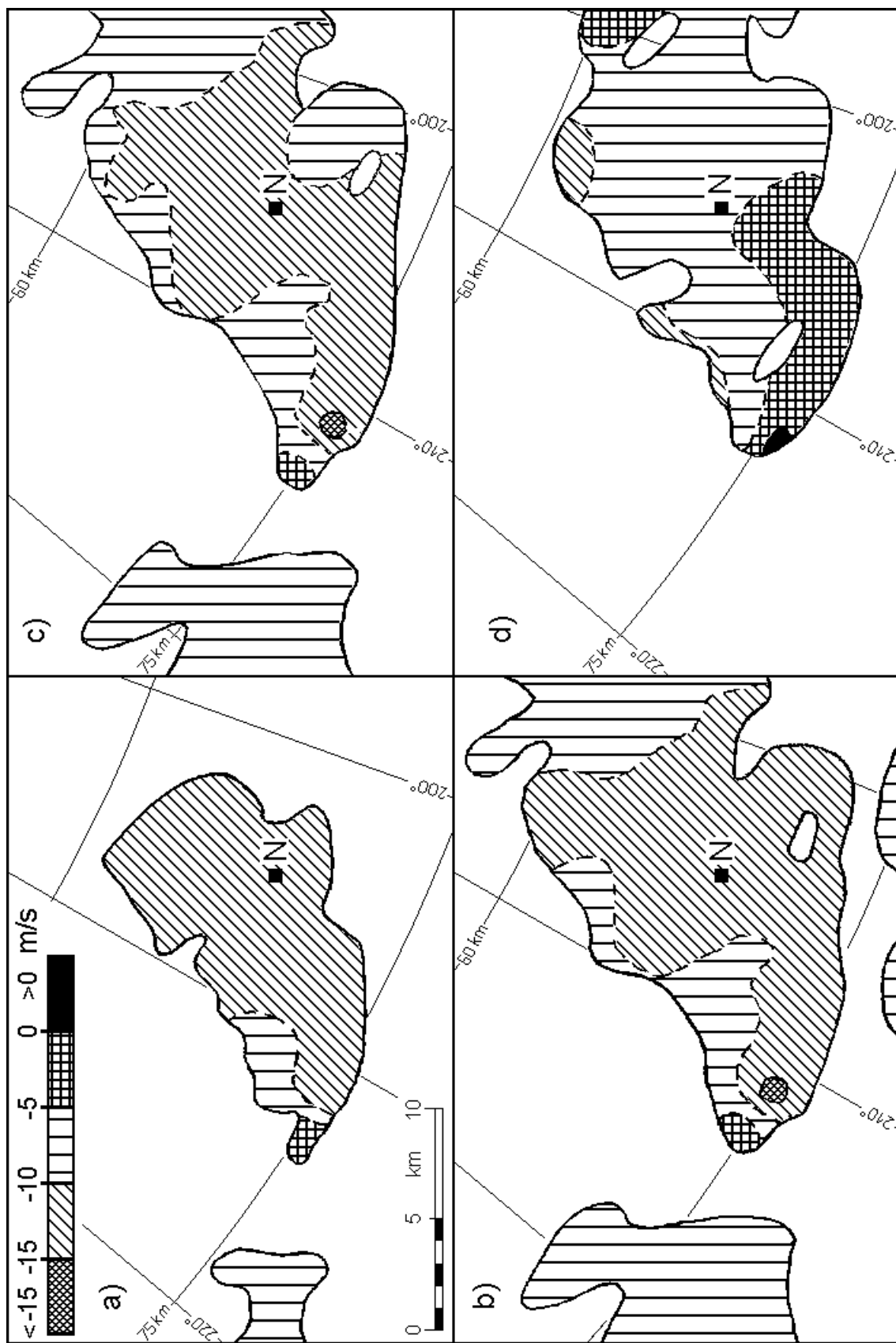


Figure 7

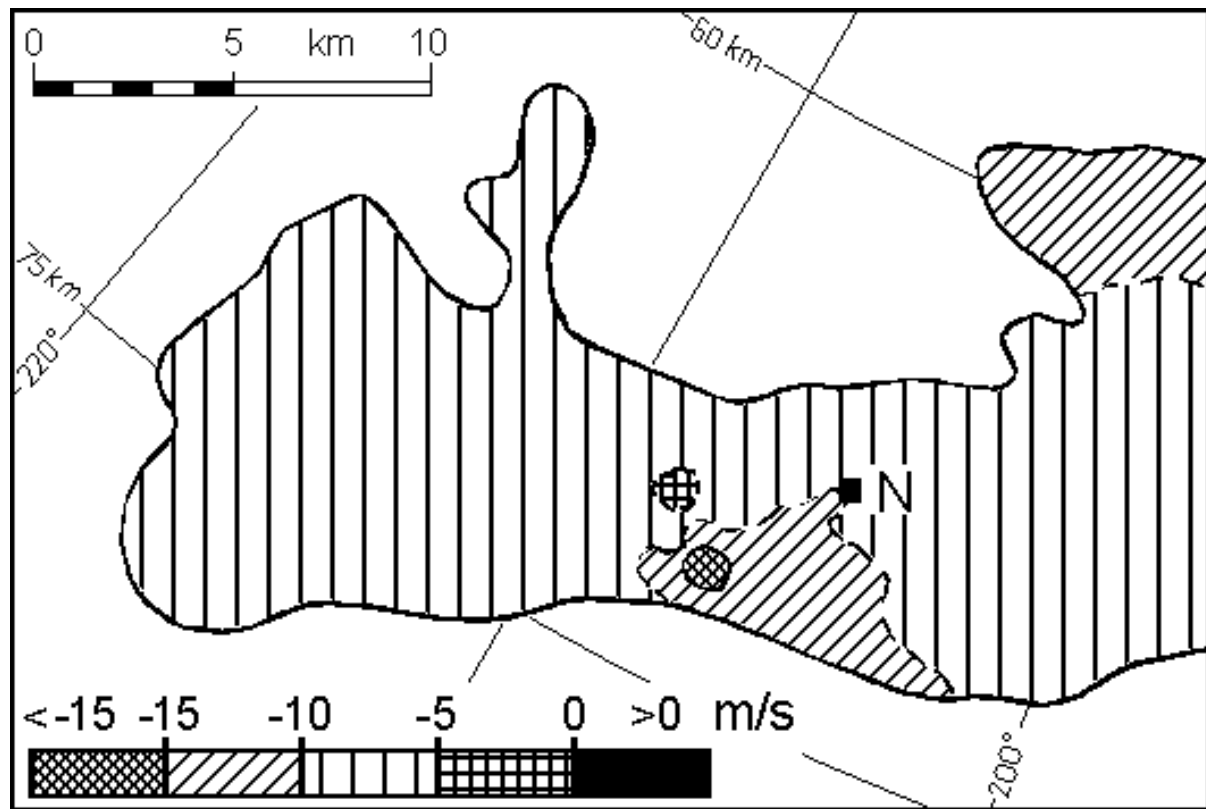


Figure 8

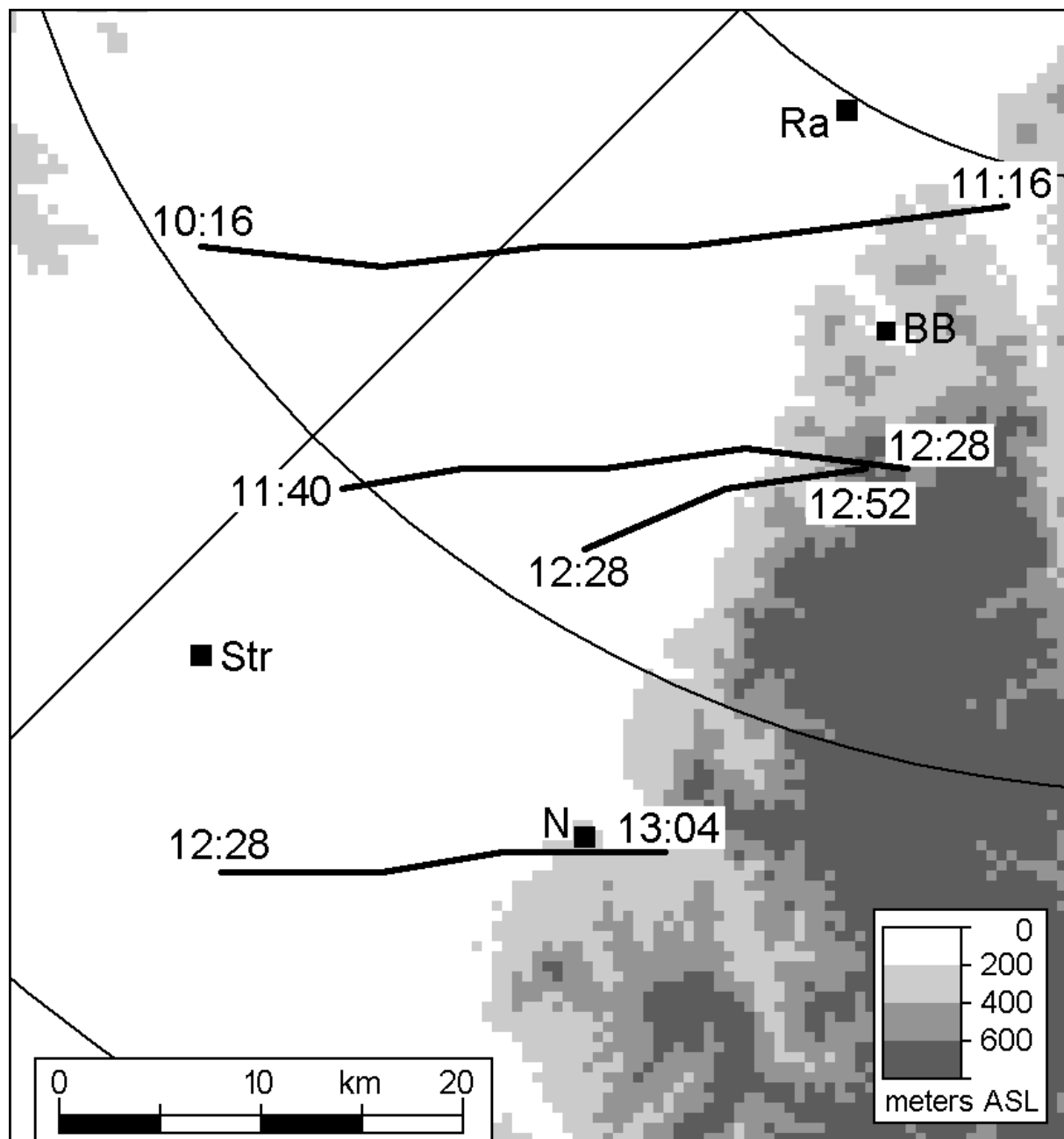


Figure 9

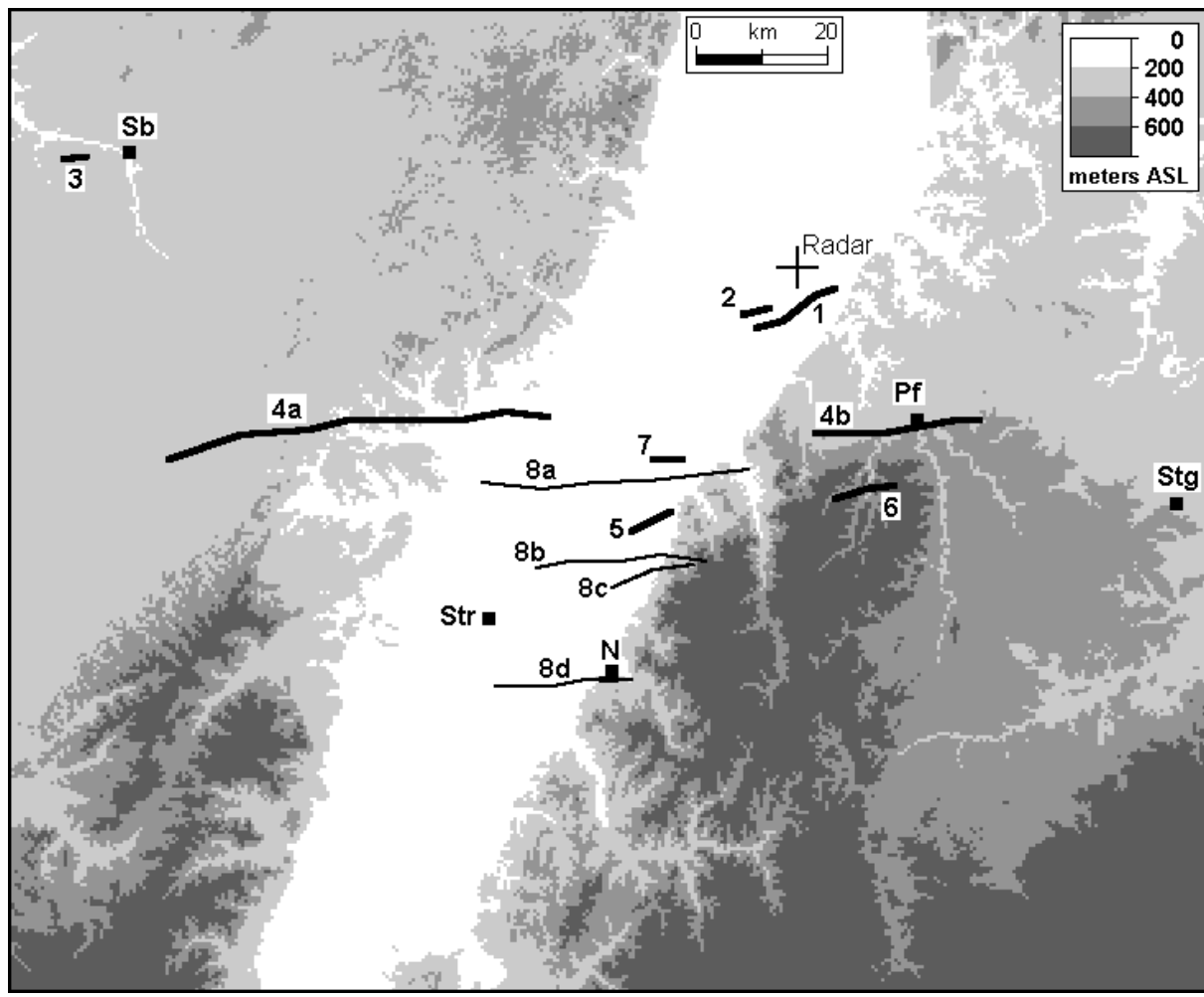


Figure 10